# Computational studies on Aerodynamic and the Strength of Material Structure of Quadcopter F3

Maria F. Soetanto,[a,*], A. Faqihan,[b] and Farhan A,[b]

[a)]*Aerodynamic Laboratory, Aeronautical Engineering, Politeknik Negeri Bandung, Indonesia*
[b)]*Aeronautical Engineering Study Program, Politeknik Negeri Bandung, Indonesia*

*Corresponding author: mariasoetanto@yahoo.com

**Paper History**

Received: 29-September-2015
Received in revised form: 18-October-2015
Accepted: 20-October-2015

## ABSTRACT

This paper focuses on the development of Quadcopter F3. Computational Fluid Dynamic (CFD) method was used to analyze the fluid flow characteristics around three main frames profiles designs, such as the lift generation for each angle of attack and longitudinal stability caused by vortex generation on trailing edge. The results show that the design of the disc-shaped main frame has an optimal aerodynamic characteristics with the value of Cl = 0.719 at 30 degrees of angle of attack and the maximum ratio Cl/Cd of 2.836. The material tensile strength test obtained that fibre carbon with epoxy resin has the optimum value of mechanical properties with tensile strength of 97.341 GPa and Modulus Young of 2140.300 GPa, while the material chosen for the frame arm analyzed through computational calculation by using the structural strength von mises stress by assuming quadcopter in maneuvering condition. The result obtained that it is safe with von mises stress of 2.769 MPa, and safety factor of 15.

**KEY WORDS:** *Quadcopter F3; Aerodynamic; Composite Material; Von Mises Stress*

## NOMENCLATURE

| | |
|---|---|
| $V$ | fluid velocity (m/s) |
| $g$ | gravity($m/s^2$) |
| $p$ | pressure (Pa) |
| T | thrust (N) |
| $F$ | force (N) |
| W | weight (N) |
| $l$ | length (m) |
| $\mu$ | dynamic viscosity |
| v | kinematic viscosity: v = $\frac{\mu}{\rho}$ |
| m | mass (kg) |
| M | momen (N.m) |
| ρ | density( $kg/m^3$) |
| A | surface area ($m^2$) |
| $v$ | free stream (m/s) |
| $c_M$ | moment coefficient |
| L | lift (N) |
| $C_l$ | lift coefficient |
| D | drag (N) |
| $C_d$ | drag coefficient |
| $\Delta L$ | Expansion |
| ε | Strain |
| σ | Stress (MPa) |
| $\sigma_v$ | von mises stress (MPa) |
| $\sigma_y$ | yield strength (MPa) |
| UAV | Unmanned Aerial Vehicle |
| CFD | Computational Fluid Dynamics |
| GAMBIT | Geometri and Mesh Building Intelegent Toolkit |

## 1.0 INTRODUCTION

Quadcopter F3 is a quadcopter that was developed by aerodynamics laboratory in aeronautical engineering study programme, mechanical engineering department of PoliteknikNegeri Bandung. It is a group of rotary wing which was given the main body on its main frame (main frame body), has

four motors are equipped with four propellers on each rotor and also with accelerometer, gyroscope and magnetometer sensors in order to control the three main variables, roll, pitch and yaw. The aim of the development of quadcopter F3, as well as on quadcopter previously developed [1,2,3,4], is for traffic monitoring, aerial surveillance, taking photos or video mapping of an area where ground transportation vehicle is considered too difficult or risky.

If on many developments of quadcopter conducted previously the stability parameter focused on the control functions and electronic sensors instruments [5,6,7,8], then in this paper the aerodynamic analysis of the fluid flow around main-frame body and the vortex formation was conducted to obtain the optimum shape of the main-frame body aerodynamics which will affect the stability factor in quadcopter. The development of a quadcopter in the ability to fly and perform its mission requires structural strength of material. Testing the tensile strength of three types of composite material performed in this paper for further analysis to obtain the optimum strength of the type of material used as a material of main-frame body, and the structure strength quadcopter also analyzed by using von mises stress criteria.

This paper discusses two important parameters in development of Quadcopter F3, first focused on the observed aerodynamics lift and drag induced by the main frame body profiles during a translational motion. Their analytic expressions play key roles in quadrotor stability and observability, then the second focused on the analysis of choice of materials and the strength of mechanical structure computational calculation.

## 2.0 BASIC THEORY

### 2.1 The Lifting Line Theory

Vortex theory was analyzed to determine the aerodynamic forces as the same as in the aerodynamic flow around 2-D section of the wing profile, lift on the main-frame body can be related to a bound circulation Γ around the main-frame body, as shown in Figure 1.

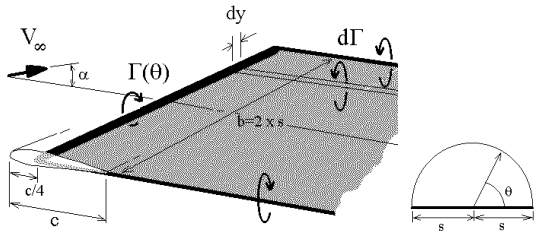


Figure 1: Wing is modeled as a single bound vortex line located at the ¼ chord position.

The vortex strength distribution in the trailing edge sheet will be a function of the changes in vortex strength along the wing span. The vortex strength is obtained by differentiating the bound vortex distribution:

$$d\Gamma = 4sV_\infty \sum_{n=1}^{\infty} nA_n \cos(n\theta) . d\theta \quad (1)$$

Where s is the wing span, θ is the twist angle and A is solution for the magnitude of the Fourier coefficients.
The lift (L) and lift coefficient ($C_L$) at a given angle of attack will be obtained by integrating the spanwise vortex distribution

$$L = \rho V_\infty \int_{-s}^{+s} \Gamma . dy \quad (2)$$

$$C_L = \pi . AR . A_1 \quad (3)$$

In the same manner, the drag (D) and drag coefficient ($C_D$) obtained:

$$D_i = \rho V_\infty \int_{-s}^{+s} \Gamma \sin(\alpha_i) . dy \quad (4)$$

$$C_{Di} = \pi . AR . \sum_{n=1}^{\infty} nA_n^2 \quad (5)$$

### 2.2. Distortion Energy Theory

The concept of Von mises stress arises from the distortion energy failure theory.According to this theory, failure occurs when the distortion energy in actual case is more than the distortion energy in a simple tension case at the time of failure.

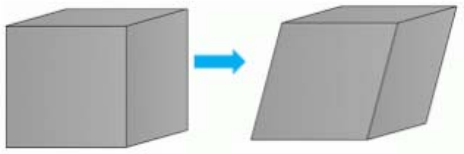

Figure 2: Representation of a pure distortion case.

Distortion energy required per unit volume, $u_d$ for a general 3 dimensional case is given in terms of principal stress values as:

$$u_d = \frac{1+\nu}{3E}\left[\frac{(\sigma_1-\sigma_2)^2+(\sigma_2-\sigma_3)^2+(\sigma_3-\sigma_1)^2}{2}\right] \quad (6)$$

Distortion energy for simple tension case is given as:

$$u_{d,sim} = \frac{1+\nu}{3E}\sigma_y^2 \quad (7)$$

The Von Misesstress is denoted as:

$$\sigma_v = \left[\frac{(\sigma_1-\sigma_2)^2+(\sigma_2-\sigma_3)^2+(\sigma_3-\sigma_1)^2}{2}\right]^{1/2} \quad (8)$$

By the von mises stress criteria, the failure condition can be expressed as:

$$\sigma_v \geq \sigma_y \quad (9)$$

## 3.0 DISCUSSION

### 3.1 Aerodynamic Calculation

A numerical calculation was conducted based on the above theory using the Fluent and GAMBIT software package. In this paper conducted an analysis of fluid flow that occur around three main-frame body design shapes: cylindrical shape, hemisphere shape, and disk shape as shown in Figure 3, to further optimization of aerodynamic characteristics obtained happens to each main-frame

body shape. The aerodynamic characteristics here are: the pressure distribution and velocity distribution that occurs lift (L) and lift coefficient ($C_L$), induced drag (D) and drag coefficient ($C_D$), ant the vortex formation that will affect the stability of the quadcopter.

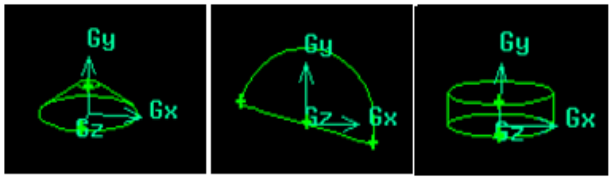


Figure 3: Three main-frame body design shapes.

There are six variations of angle of attack given in this calculation, i.e.: AOA = $0^o$, $15^0$, $30^0$, $45^0$, $60^0$, and $90^0$.

The first investigation conducted was the pressure distribution and velocity distribution that occur on the lower surface and upper surface of each design of main frame body shape. These results are shown from Figure 4 to Figure 6.

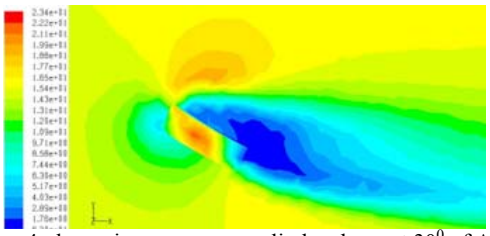

Figure 4: dynamic pressure on cylinder shape at $30^0$ of AOA

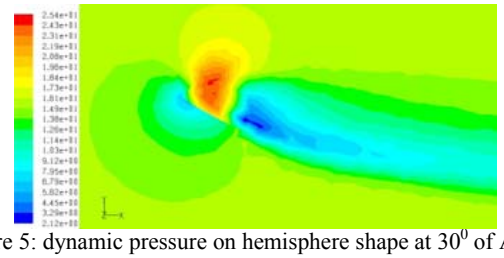

Figure 5: dynamic pressure on hemisphere shape at $30^0$ of AOA.

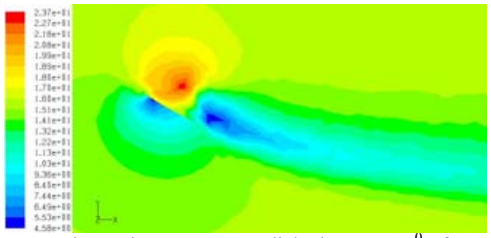

Figure 6: dynamic pressure on disk shape at $30^0$ of AOA.

Analysis for this is as follows: the maximum pressure difference, Δp, that occurs on the main-frame body in the shape of disk is equals to 18.77 Pa, Δp = 22.38 Pa generated from a hemisphere shape of main-frame body, whereas in the cylinder shape of main-frame body, the maximum different pressure generated by 39 Pa. This means that the cylinder shape profile creates more lift for angle of attack of $30^0$, but also that the stall angle of attack is lower. On the contrary, to the disk shape, the pressure difference obtained less, so that the lift force generated will also be lower, which will delay the occurrence of stall condition.

Figure 7 to Figure 9 shown the y-velocity distributions of around three main-frame body shapes at $0^0$ of angle of attack.

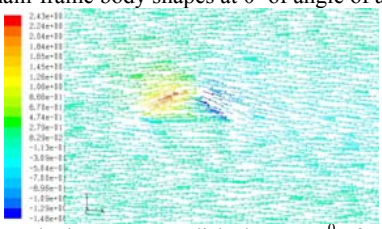

Figure7: Velocity vector on disk shape at $0^0$ of AOA.

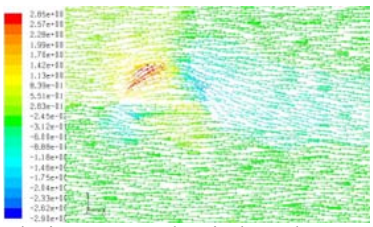

Figure 8: Velocity vector on hemisphere shape at $0^0$ of AOA.

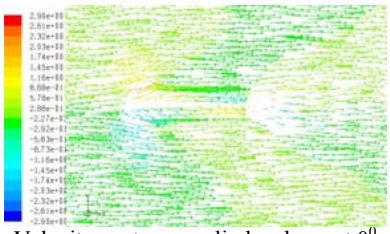

Figure 9: Velocity vector on cylinder shape at $0^0$ of AOA.

The velocity vector of the simulation results shows that the maximum fluid velocity occurs at the main-frame body of a cylinder shape which amounted of 2.91 m/s, then in the hemisphere shape has a maximum velocity of 2.65 m/s, and the lowest, i.e. $V_y$ = 2.43 m/s generated by disc shape of main-frame body. This means that the maximum induced drag occurs in a cylinder shape while the main-frame body which the disc shape has the smallest induced drag. Analysis of it is also reinforced by the formatting of vortices that occurs on the trailing edge of each shape of main-frame body, as shown from Figure 10 to Figure 12 below:

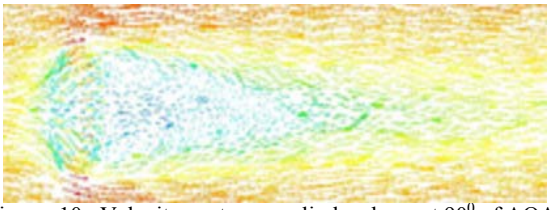

Figure 10: Velocity vector on cylinder shape at $90^0$ of AOA.

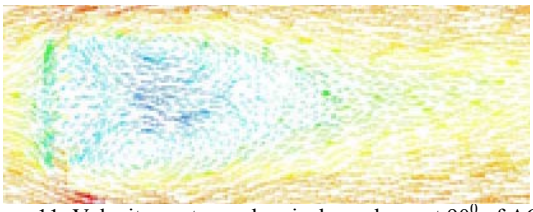

Figure 11: Velocity vector on hemisphere shape at $90^0$ of AOA.

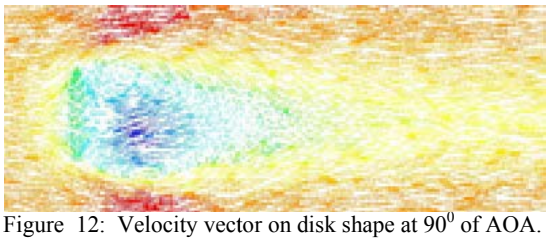

Figure 12: Velocity vector on disk shape at $90^0$ of AOA.

Vortex formation caused by turbulent flow that occurs at the rear main-frame body leads to the released energy. The greater the energy released, the longer the formation of vortex formed. It is seen that the disk shape of main-frame body has a shorter vortex formation, that means it has the most optimal aerodynamic characteristics due to induced drag generated by the disk shape of main-frame body is the minimal.

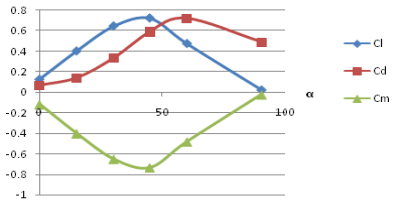


Figure 13: Cl, Cd and Cm vs AOA on disk shape.

Therefore, the development of Quadcopter F3 in this paper used disk shape main-frame body. Figure 13 above shows the results of calculation of aerodynamic coefficients generated by disc shape of main-frame body at various angles of attack

### 3.2 Tensile Testing

Tensile test performed on three variations of composite materials: carbon fiber epoxy resin, fiberglass epoxy resin, and fiberglass polyester resin. The results are shown in Table 1 below:

Table 1: Results of 3 different variations of composite materials

| No. | Material | Force @ Peak (N) | Young's modulus (Pa) | Tensile Strength (Pa) | Strength @ break (Pa) | Elongation percentage @ break (%) | Elongation percentage @ peak (%) |
|---|---|---|---|---|---|---|---|
| 1 | Fiberglass resin polyester | 791.180 | 1499639694.395 | 72852663.723 | 72371993.392 | 5.618 | 5.587 |
| 2 | Fiberglass resin epoxy | 583.788 | 688491573.503 | 58754822.179 | 57897825.984 | 7.826 | 7.787 |
| 3 | Fiber carbon resin epoxy | 829.113 | 1425419485.834 | 75223464.970 | 70750682.334 | 7.114 | 7.047 |
| 4 | Fiberglass resin epoxy | 246.384 | 1166098738.910 | 44610580.469 | 43588188.821 | 4.854 | 4.825 |
| 5 | Fiber carbon resin epoxy | 728.307 | 2140300607.388 | 97341159.167 | 85403181.506 | 5.983 | 5.911 |
| 6 | Fiberglass resin polyester | 198.182 | 1515248262.541 | 11731581.672 | 6206872.776 | 1.665 | 1.350 |
| Max | | 829.113 | 2140300607.388 | 97341159.167 | 85403181.506 | 7.826 | 7.787 |
| Min | | 198.182 | 688491573.503 | 11731581.672 | 6206872.776 | 1.665 | 1.350 |
| Mean | | 562.826 | 1405866393.762 | 60085712.030 | 56036457.469 | 5.510 | 5.418 |

From the data test results, the carbon fiber with epoxy resin is used as a main-frame body material.

### 3.1 Von Mises Stress Calculation

Von mises stress criteria is used in this paper to analyze the strength of material structure quadcopter by using Ansys software. In this calculation, quadcopter assumed to be in a state of maneuver. there are nine loads givenas initial condition on simulation calculations, where eight loads, which is assumed to be thrust motors of 2.085 N, is applied at the tip of frame arm, and one load of 13.72 N, which is assumed as the netted weight of quadcopter (without motors), is given to the main frame. The results are:

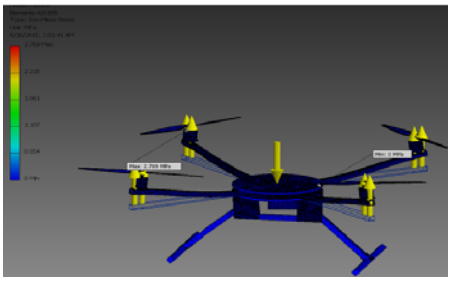

Figure 14: Von Mises Stress of frame arm

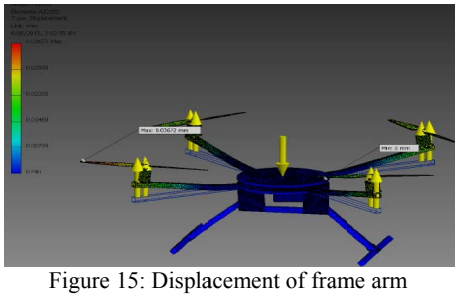

Figure 15: Displacement of frame arm

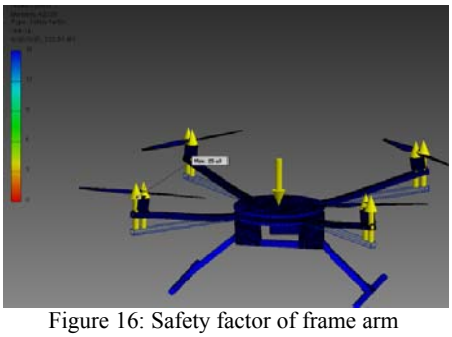

Figure 16: Safety factor of frame arm

As shown in Figure 14, von mises stress of quadcopter on maneuver condition obtained at 2.769 MPa, the value of displacement maximum, as shown in Figure 15, amounted to 0.037 mm, while the safety factor obtained exist on a scale of 15, as shown in Figure 16, this means that the structure of quadcopter F3 is in a safe condition.

## 4.0 MANUFACTURING AND FLIGHT TEST

### 4.1 Manufacturing and Assembling

Once obtained optimization computational calculations, then performed the manufacturing of components quadcopter F3. Assembling process is then performed. The results are shown in Figure 17 below:

Figure 17: Assembling Quadcopter components.

### 4.2 Flight Test

Before carrying out the flight test, first the condition of Quadcopter F3. Checks carried out on electrical components, such as electronic speed controller (ESC), GPS, flight control, brushless motor, so that all electrical components can function as it should. The next is checked the range of remote control against the quadcopter ability to fly. After the checking is done, then the flight test can be carried out. Figure 18 shows the Quadcopter F3 has be able to fly and performs several maneuvers to fly.

Figure 18: Flight test

## 5.0 CONCLUSION

The development Quadcopter F3 in this paper using the main-frame body in the form of disk shape with maximum ratio $C_L/C_D$ of 2.837 at angle of attack of $30^0$, with the composite material of carbon fiber epoxy resin. The strength of the structure based on the Von Mises stress criteria has been validated safe with safety factor = 15 and the ability to fly of quadcopter has been tested by performing a test flight.

## ACKNOWLEDGEMENTS

The authors would like to convey a great appreciation to Aerodynamic laboratory Aeronautical Engineering Study Programme Mechanical Engineering Department Politeknik Negeri Bandung for supporting this research.

## REFERENCE

1. D. Greer, P. McKerrow, and J. Abrantos (2002). *Robots in Urban Search and Rescue Operations*, Australian Conference on Robotics and Automation, Auckland.
2. Y. Naidoo, R. Stopforth, and G. Bright (2011), *Development of UAV for Search and Rescue Application*, IEEE Africon, Zambia.
3. G. Hoffmann, H. Huang, S. Waslander, and C. Tomlin (2007). Proceedings of the AIAA Guidance, Navigation, and Control Conference, Hilton Head.
4. P.Pounds, J. Gresham, R. Mahony, J.Robert, and P.Corke (2006). *Modelling and Control of a Quad-rotor Robot.* Proceedings of the Australian Conference on Robotics and Automation, Auckland, New-Zealand.
5. A. Tayebi and S. McGilvray (2006). *Attitude stabilization of a VTOL quadrotor aircraft*. IEEE Transactions on Control System Technology, vol. 14, no.3, pp. 562-571.
6. H. Romero, S.Salazar, A. Sanchez, P.Castillo, and R. Lozano (2007).*Modelling and real-time control stabilization of a new VTOL aircraft with eight rotors*. IEEE International Conference Intelligent Robotics and Automation.
7. D. Vissiere, P.J. Bristeau, A. Martin, and N. Petit (2008).

*Experimental autonomous flight on a small-scaled helicopter using accurate dynamics model and low-cost sensors*. Proceeding of the 17th HAC World Congress, Seoul, Korea.

8. H. Huang, G.M. Hoffman, S.L. Waslander, and C. Tomlin, "Aerodynamics and control of Autonomous Quadrotor Helicopters in Aggressive Manoeuvring", IEEE International Conference Intelligent Robotics and Automation, Japan, 2009.
9. P.Pounds, and R. Mahony(2009). *Design principles of large quadrotors for practical applications*. Proceedings of the IEEE International Conference on Robotics and Automation (ICRA), pp.3265 – 3270.
10. P.Pounds, and R. Mahony (2010). *Modelling and Control of a Large Quadrotor Robot.* Control Engineering Practice, vol.18, pp. 691 – 699.